NANO LETTERS

LETTER

pubs.acs.org/NanoLett

Optimization of Band Structure and Quantum-Size-Effect Tuning for Two-Photon Absorption Enhancement in Quantum Dots

Lazaro A. Padilha,[†] Gero Nootz,[†,‡] Peter D. Olszak,[†] Scott Webster,[†] David J. Hagan,[†,‡] Eric W. Van Stryland,[*,†,‡] Larissa Levina,[§] Vlad Sukhovatkin,[§] Lukasz Brzozowski,[§] and Edward H. Sargent[§]

[†]CREOL: The College of Optics and Photonics and [‡]Physics Department, University of Central Florida, 4000 Central Florida Boulevard, Orlando, Florida 32826, United States

[§]The Edward S. Rogers Sr. Department of Electrical and Computer Engineering, University of Toronto, Toronto, ON, Canada, M5S3G4

ABSTRACT: The two-photon absorption, 2PA, cross sections of PbS quantum dots, QDs, are theoretically and experimentally investigated and are shown to be enhanced with increasing quantum confinement. This is in contrast to our previous results for CdSe and CdTe QDs where the reduced density of states dominated and resulted in a decrease in 2PA with a decrease in QD size. Qualitatively this trend can be understood by the highly symmetric distribution of conduction and valence band states in PbS that results in an accumulation of allowed 2PA transitions in certain spectral regions. We also measure the frequency nondegenerate 2PA cross sections that are up to five times larger than for the degenerate case. We use a $\boldsymbol{k}\cdot\boldsymbol{p}$ four-band envelope function formalism to model the increasing trend of the two-photon cross sections due to quantum confinement and also due to resonance enhancement in the nondegenerate case.

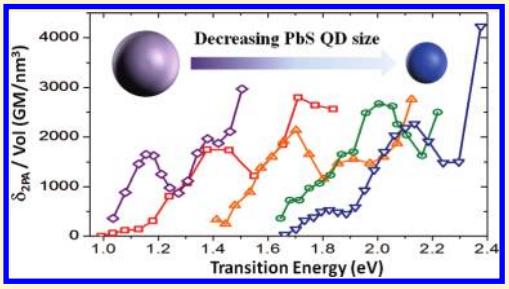

KEYWORDS: Nonlinear optics, two-photon absorption, quantum dots, nonlinear spectroscopy, lead salt, band structure

Studied for many years, two-photon absorption,[1−4] 2PA, with additional enhancements will lead to both improvements in current[1−5] and unforeseen applications. Semiconductor quantum dots, QDs, emerged as promising candidates for 2PA enhancement after early predictions indicated increasing nonlinearities with decreasing QD size.[6−8] However, it has been recently shown that the 2PA cross-section in CdSe and CdTe decreases for smaller QD sizes due to their decreasing density of states.[9−11]

The first reports on 2PA cross sections, δ_{2PA}, of colloidal CdSe QDs[1,12] exhibited values larger than 10,000 GM (1 GM = 10^{-50} cm^{4}s); however, the 2PA decreased for smaller QDs.[1,13] Our studies revealed that δ_{2PA} of CdSe and CdTe QDs decrease for smaller QDs even after being normalized by the volume of the QDs, and they are less than the value for an equivalent volume of bulk semiconductor.[9,10] This is explained by the decrease in the density of states with increasing quantum confinement that more than compensates the increasing oscillator strength of a single two-photon transition as the QD is reduced in size.[9−11]

The unusual band structure of the lead salts, with similar effective masses of electrons and holes, results in a symmetric distribution of the quantum-confined energy levels in the valence and conduction bands. This in turn leads to transitions confined to narrow energy regions. Additionally, due to the small bulk bandgap energy (E_g^{Bulk}), the density of states is nearly constant in terms of the QD bandgap energy (E_g) for $E_g \gg E_g^{Bulk}$, that is, the transitions remain densely packed within narrow energy regions as the size of the QDs is reduced. Figure 1 illustrates the differences between CdSe and PbS QDs by comparing the calculated spectral spreading of the 2PA transitions.

Furthermore, these properties of the PbS band structure make the intraband transition energies comparable to E_g for highly confined QDs. Since 2PA transitions are composed of one-photon absorption (1PA) allowed transitions, such large intraband transition energies can lead to strong enhancement of the δ_{2PA} for slightly frequency-nondegenerate photons due to intermediate state resonance enhancement (ISRE).[9,10,14]

Here we show for the first time quantum confinement enhancement of two-photon absorption in semiconductors. In other words, we demonstrate that for PbS QDs the volume normalized 2PA is higher in small QDs as compared to larger ones. We account for this much-needed enhancement in nonlinear performance of the materials through a combination of strong quantum confinement and highly symmetric distribution of conduction and valence band states in PbS quantum dots that results in an accumulation of allowed two-photon transitions in narrow spectral regions. Additionally, we studied the frequency-nondegenerate 2PA and observe up to a five times increase in 2PA compared to the frequency degenerate case due to ISRE.[9,10,14] Using a $\boldsymbol{k}\cdot\boldsymbol{p}$ four-band envelope function formalism[15] to describe the quantum dots eigenfunctions, we predict the observed increasing trend of the two-photon absorption cross sections from quantum confinement in the degenerate case and from quantum confinement and resonance enhancement in the nondegenerate case.

Received: December 3, 2010
Revised: January 26, 2011
Published: February 11, 2011

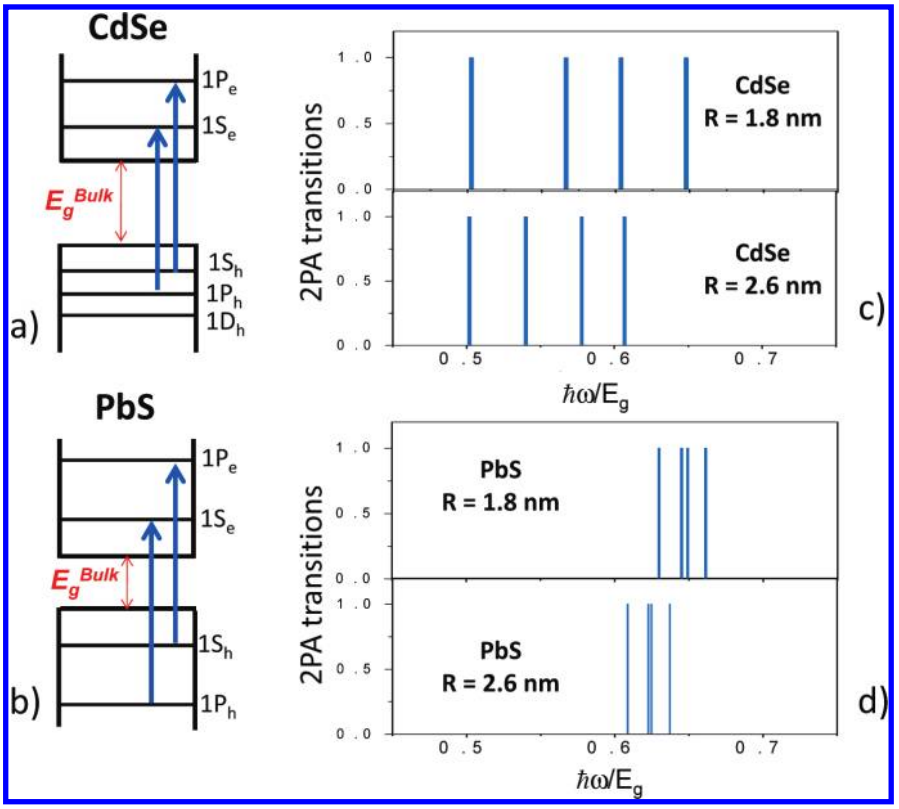

Figure 1. Schematic of the band structure for (a) CdSe and (b) PbS QDs. E_g^{Bulk} is much larger for CdSe than PbS, additionally PbS QDs have a more symmetric distribution of quantum confined levels than CdSe. The energy of the four first allowed 2PA transitions for (c) CdSe and (d) PbS are shown for two sizes of QDs, demonstrating the larger spectral spreading due to quantum confinement in CdSe than in PbS. Note also that the first parity-allowed 2PA transition is closer to QD band edge $(\hbar\omega)/E_g = 0.5$ in CdSe than in PbS QDs, which is a result of the high energy of the intraband transitions in PbS and can lead to strong IRSE for 2PA.

Our measurements are performed using several sizes of oleic-acid capped colloidal PbS QDs grown as described in ref 16 and dispersed in toluene. The nomenclature we adopt to identify the QD studied is related to the position of its $1S_h \rightarrow 1S_e$ peak, for example, PbS-1123 refers to the QD sample with its $1S_h \rightarrow 1S_e$ peak at 1123 nm. The concentration of the colloidal PbS QDs is estimated using the empirical method proposed by Cademartiri et al.[17]

The two-photon spectroscopy is performed using optical parametric generators/amplifiers, OPG/OPA's, tunable from 300 nm to 11 μm (TOPAS-800) pumped at 780 nm, 140 fs pulses from a Ti:Sapphire regenerative amplifier (Clark-MXR, model CPA 2010) operating at a 1 kHz repetition rate. All samples are investigated at room temperature. The frequency-degenerate 2PA spectrum is obtained by two-photon excited fluorescence (2PF)[18] and open-aperture Z-scan.[19] Because of the detection system of the spectrofluorometer (PTI) our 2PF measurements are limited to samples with fluorescence at wavelengths shorter than 800 nm. For samples with fluorescence at wavelengths longer than 800 nm, the entire spectrum is measured by the Z-scan technique. The Z-scan calibration is verified by using standard two-photon absorbers (bulk CdTe, GaAs and GaSb), and carbon disulfide (CS_2) which is a standard nonlinear refractive material. The detectors used in the Z-Scan experiment are home-built Si and Ge based photodiodes for wavelengths up to 1.7 μm and Thorlabs PDA30G PbS detectors for longer-wavelength measurements.

Figure 2 shows the degenerate 2PA spectrum measured by 2PF[18] and open-aperture Z-Scan.[19] The values shown are corrected by the local field penetration, f, using the Maxwell-Garnett model.[20] Because of the high dielectric constants of PbS, $f \sim 0.36$ for the studied colloidal QDs.[21] The QD radii indicated are estimated from the four-band envelope function formalism developed by Kang and Wise.[15] For each sample the 2PA spectrum is composed of at least two 2PA peaks; however, only the peaks indicated by the arrow in Figure 2a, corresponding to the $1S_h \rightarrow 1P_e$ and $1P_h \rightarrow 1S_e$ transitions, are parity-allowed according to the four-band envelope function formalism, and those are the transitions discussed in this paper. As we have shown elsewhere,[22] the other observed 2PA transitions occur at the energies of 1PA allowed transitions where, due to asymmetry introduced by the strong quantum confinement, 2PA transitions also become allowed. The energies of the next parity allowed 2PA transitions, $1P_h \rightarrow 1D_e$ and $1D_h \rightarrow 1P_e$, lie above $2 \times E_g$ and are experimentally inaccessible since frequency-degenerate 2PA spectroscopy is limited to photon energies $1/2\ E_g < \hbar\omega < E_g$.

The magnitude of the 2PA at the parity-allowed 1Sh→1Pe and 1Ph→1Se transitions strongly decreases as the QD size is reduced, ranging from 126 000 to 30 500 GM (±15%). This trend is expected based on the difference in the QD volume. However, it is more appropriate to compare the magnitude of the 2PA for different QD sizes by calculating the volume normalized 2PA. These are shown in Figure 2b, indicating that the trend of the 2PA dependence on the QD size is reversed. For the first 2PA parity allowed peak, the volume normalized δ_{2PA} increases from 1680 GM/nm^3 for PbS-1335, to 2700 GM/nm^3 for PbS-780. The volume normalized 2PA cross-section for PbS-740 decreases to 2220 GM/nm^3. This size dependence of the volume

dx.doi.org/10.1021/nl1042209 |*Nano Lett.* 2011, 11, 1227–1231

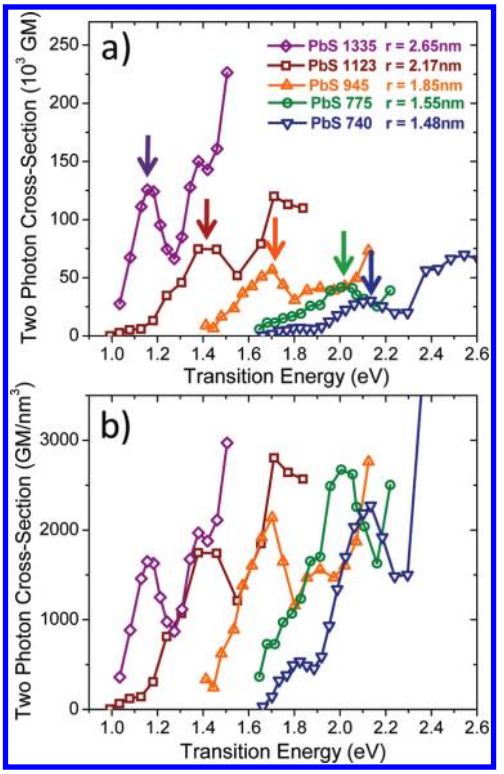

Figure 2. (a) 2PA cross section spectra for PbS QDs. The arrows indicate the parity allowed $1S_h \rightarrow 1P_e$ and $1P_h \rightarrow 1S_e$ transitions. (b) Same as in panel (a) for the volume normalized 2PA cross section.

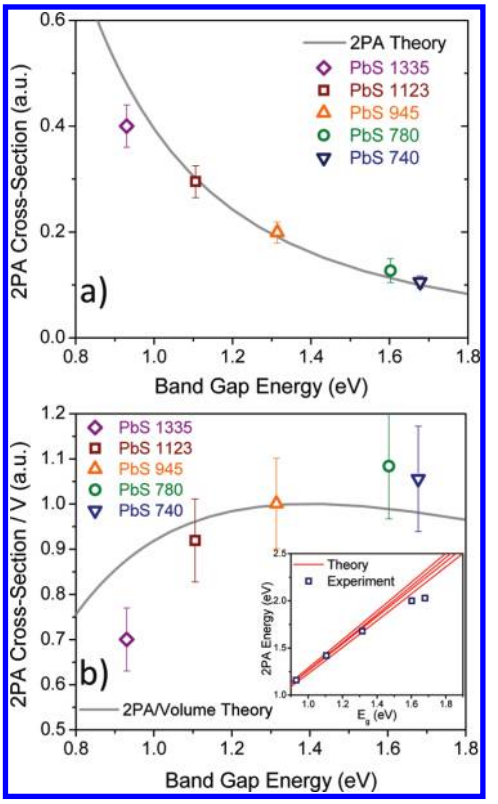

Figure 3. Comparison of the experimental (a) 2PA cross section and (b) volume normalized 2PA cross section versus bandgap energy to the predictions of the 2PA calculated using the QD wave functions obtained by the four-band envelope function formalism.[15] The inset in (b) shows the predicted 2PA $1P_h \rightarrow 1S_e$ and $1S_h \rightarrow 1P_e$ transition energy and the position of the measured 2PA peak versus E_g.

normalized δ_{2PA} is opposite to the trend previously observed for II−VI semiconductor QDs.[9−11]

To explain the observed trend for 2PA in PbS QDs, we calculate the size dependent energy and oscillator strength of the parity-allowed 2PA transitions using the four-band envelope function formalism.[15] In this model, the QDs are assumed to be spheres with infinite potential barriers, and the eigenstates are constructed by considering the mixing of the first valence and conduction bands. The details of the four-band envelope formalism are described in ref 15. In summary, the resulting eigenstates have well-defined parity, π, leading to strict selection rules for 1PA and 2PA transitions. The spherical symmetry of the model predicts states which are energy degenerate in the z-projection of the total angular momentum, m. For simplicity, we label the eigenstates using the typically used nomenclature ($1S_{h,e}$, $1P_{h,e}$, $1D_{h,e}$, $nS_{e,h}$, etc.), where S, P, and D correspond to the value of the angular momentum l of the dominant term in the mixed wave functions of the quantum confined state and n corresponds to the order of the wave function. Since here we are investigating nonresonant nonlineatires, that is, transitions caused by photons with energy below the bandgap (transition energies below $2 \times E_g$), in the modeling, the sum over intermediate states can be truncated at $n \leq 5$ without changing the results by more than 1%.

The most general form to describe two-photon transition rates is given by[9,10,23]

$$W(\omega_1, \omega_2) = \frac{2\pi}{\hbar} \sum_{v,c} |M_{v,c}|^2 \delta(E_c - E_v - \hbar\omega_1 - \hbar\omega_2) \quad (1)$$

where $\hbar\omega_1$ and $\hbar\omega_2$ are the energies of the photons involved in the process. The 2PA oscillator strength for a transition between the initial state in the valence band and the final state in the conduction band, $M_{v,c}$, is given by[10]

$$M_{v,c} = \frac{1}{2} \sum_i \frac{\langle \psi_c | \vec{e}_1 \cdot \vec{p} | \psi_i \rangle \langle \psi_i | \vec{e}_2 \cdot \vec{p} | \psi_v \rangle}{E_i - E_v - \hbar\omega_1} + \frac{\langle \psi_c | \vec{e}_2 \cdot \vec{p} | \psi_i \rangle \langle \psi_i | \vec{e}_1 \cdot \vec{p} | \psi_v \rangle}{E_i - E_v - \hbar\omega_2} \quad (2)$$

The intermediate states, $|\Psi_i\rangle$, are all the one-photon accessible states in the valence or conduction bands. Thus, a two-photon transition is composed of an intraband and an interband transition, obeying parity selection rules opposite from the 1PA transitions. The δ_{2PA} is defined by

$$\delta_{2PA}(\omega_1, \omega_2) = \frac{\kappa}{\hbar\omega_1 \hbar\omega_2} W^{(2)}(\omega_1, \omega_2) \quad (3)$$

where κ is a size-independent constant.

Figure 3a shows the calculated size dependence of the parity-allowed $1S_h \rightarrow 1P_e$ and $1P_h \rightarrow 1S_e$ 2PA transitions compared to the experimental values. To account for the different size distributions of the QDs, the theoretical predictions are compared to the integrated 2PA under the $1S_h \rightarrow 1P_e$ and $1P_h \rightarrow 1S_e$ peaks, showing good agreement. Also, after normalizing the δ_{2PA}s by the QD volume (Figure 3b), we see good qualitative agreement with the experimental results. The model predicts that the volume normalized 2PA of the first group of allowed transitions should reach a maximum for QDs having a bandgap energy of ~1.4 eV; however, experimentally we do not observe this maximum of the

dx.doi.org/10.1021/nl1042209 |Nano Lett. 2011, 11, 1227–1231

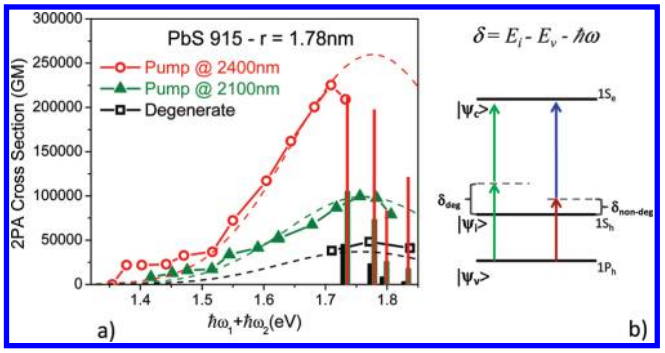

Figure 4. (a) Degenerate vs nondegenerate 2PA cross sections measured for PbS-915. The vertical lines indicate the predicted transitions using eq 2 and the four-band envelope function formalism.[15] The different colors indicate the different degrees of nondegeneracy: black for degenerate, green for pump at 2100 nm, and red for pump at 2400 nm. The oscillator strength for each transition is indicated by the height of the lines. The fittings, indicated by the dashed line, are done using the magnitude calculated and the inhomogeneous broadening due to the size distribution (±5%). (b) The enhancement is explained by the decreasing of the detuning energy, $\delta = E_i - E_v - \hbar\omega$ for the nondegenerate case.

volume normalized 2PA for QDs with bandgap energies up to ~1.6 eV. Only the smallest QDs studied in this work, with a bandgap of 1.78 eV, have a smaller volume normalized 2PA than slightly larger QDs. This may indicate that the volume normalized 2PA maximum has been reached. PbS QDs with larger bandgap energies could not be studied due to difficulties with the synthesis of smaller, stable, QDs with sufficiently narrow size distributions. The experimental results show slightly stronger 2PA enhancement than that theoretically predicted for the range of QDs studied and a shift of the maximum volume normalized 2PA to QDs with higher E_g (Figure 3b). These discrepancies can be explained by the overestimation of the 2PA transition energies for small QDs by the four-band envelope formalism that considers infinite confinement potentials.[15] The inset of Figure 3b shows the predicted energies of the transitions corresponding to the $1S_h \rightarrow 1P_e$ and $1P_h \rightarrow 1S_e$ peaks and the peak position measured experimentally. The divergence between the theoretical and experimental values occurs only for the smallest QDs. From eq 3, the overestimation of the transition energy leads to an underestimation of the δ_{2PA}, which explains the small difference between the predicted and experimentally observed enhancement of the volume normalized 2PA (Figure 3b).

For QDs with $E_g \sim 1$ eV or larger, the intraband transition energy between 1P and 1S levels is not negligible if compared to E_g, $E_{1Se \rightarrow 1Pe} \sim 1/4E_g$. These intraband transitions correspond to the intermediate transitions for the $1S_h \rightarrow 1P_e$ and $1P_h \rightarrow 1S_e$ 2PA (see eq 2). Because of ISRE one would expect to obtain strong 2PA enhancement for the $1S_h \rightarrow 1P_e$ and $1P_h \rightarrow 1S_e$ transitions by using frequency-nondegenerate photons without the need of highly nondegenerate photon pairs.

The frequency-nondegenerate 2PA spectroscopy is performed using pump-probe experiment as described in ref 24. In brief, the pump is selected from one OPG/OPA and the probe is selected from a white-light continuum generated in a CaF_2 crystal pumped at 1300 nm selected from a second OPA. For the strong pump, the photon energy is chosen such that $\hbar\omega_1 < 1/2E_g$ to avoid degenerate 2PA from the pump beam. The weak probe has photon energies in the range $1/2E_g < \hbar\omega_2 < E_g$. The analysis of the 2PA is done following the model described in ref 24.

Figure 4a shows the nondegenerate 2PA spectra for excitation at two different wavelengths, 2100 nm ($\hbar\omega_1 = 0.44 \times E_g$) and 2400 nm ($\hbar\omega_1 = 0.38 \times E_g$), for sample PbS-915 and the degenerate 2PA measured via Z-scan at the $1S_h \rightarrow 1P_e$ and $1P_h \rightarrow 1S_e$ peak. Also shown in Figure 4a are the theoretically predicted δ_{2PA} for the degenerate and nondegenerate cases. An enhancement factor of ~2.5 and ~5 for the 2PA peak measured for excitation at 2100 and 2400 nm, respectively, is observed if compared to the degenerate 2PA values. The measured enhancement agrees with the ISRE predicted using the four-band envelope formalism.

The maximum enhancement observed for PbS QDs at the first 2PA peak is ~3× larger than that observed for CdSe QDs under similar ratios of nondegeneracy ($\hbar\omega_1 = 0.39 \times E_g$).[10] This is a consequence of the stronger quantum confinement in PbS QDs. The energy of the intraband $1S_e \rightarrow 1P_e$ in PbS is $\sim 1/4E_g$. For CdSe QDs, this ratio is twice as small, consequently the ISRE in CdSe is considerably smaller. To obtain a similar enhancement in CdSe, the ratio between photon energies ($\hbar\omega_1/\hbar\omega_2$) would need to be approximately twice as large as that used here.

In conclusion, our analysis of the size dependent δ_{2PA} in PbS QDs shows that quantum confinement enhances the volume normalized δ_{2PA} for smaller PbS QDs, reaching a maximum value for QDs with bandgaps of ~1.67 eV. Using a four-band envelope formalism,[15] we calculate the size dependence of the 2PA transition energy and oscillator strength for the parity-allowed $1S_h \rightarrow 1P_e$ and $1P_h \rightarrow 1S_e$ two-photon transitions, showing that the enhancement of the 2PA is due to the unusual band structure of PbS, which has a small bulk bandgap energy and very symmetric conduction and valence bands with nearly identical small effective masses. Furthermore, the resulting large energies for the intraband transitions ($E_{1Se \rightarrow 1Pe} \sim 1/4E_g$) allows for strong intermediate-state resonance enhancement using only slightly nondegenerate photons. This makes PbS QDs promising candidates for applications in 2PA based devices. The same 2PA enhancement is expected for any material engineered with similar band structure.

AUTHOR INFORMATION

Corresponding Author
*E-mail: ewvs@creol.ucf.edu.

ACKNOWLEDGMENT

This work is supported in part by the U.S. Army Research Office under Contract/Grant 50372-CH-MUR, the Air Force Office of Sponsored Research MURI AFOSR grant FA9550-06-1-0337, the DARPA ZOE program Grant W31R4Q-09-1-0012, the Israel Ministry of Defense Contract 993/54250-01, and by the Natural Sciences and Engineering Research Council of Canada (NSERC) and the Ontario Research Fund.

REFERENCES

(1) Larson, D. R.; Zipfel, W. R.; Williams, R. M.; Clark, S. W.; Bruchez, M. P.; Wise, F. W.; Webb, W. W. *Science* **2003**, *30*, 1434.
(2) Hales, J. M.; Matichak, J.; Barlow, S.; Ohira, S.; Yesudas, K.; Brédas, J. L.; Perry, J. W.; Marder, S. R. *Science* **2010**, *327*, 1485.
(3) Resch-Genger, U.; Grabolle, M.; Cavaliere-Jaricot, S.; Nitschke, R.; Nann, T. *Nat. Methods* **2008**, *5*, 763.

(4) Dhenaut, C.; Ledoux, I.; Samuel, I. D. W.; Zyss, J.; Bourgault, M.; Le Bozec, H. *Nature* **1995**, *374*, 339.
(5) Nozaki, K.; Tanabe, T.; Shinya, A.; Matsuo, S.; Sato, T.; Taniyama, H.; Notomi, M. *Nat. Photonics* **2010**, *4*, 477.
(6) Roussignol, P.; Ricard, D.; Flytzanis, C. *Appl. Phys. B* **1990**, *51*, 437.
(7) Kataoka, T.; Tokizaki, T.; Nakamura, A. *Phys. Rev. B* **1993**, *48*, 2815.
(8) Schmitt-Rink, S.; Miller, D. A. B.; Chemla, D. S. *Phys. Rev. B* **1987**, *35*, 8113.
(9) Padilha, L. A.; Fu, J.; Hagan, D. J.; Van Stryland, E. W.; Cesar, C. L.; Barbosa, L. C; Cruz, C. H. B. *Opt. Express* **2005**, *13*, 6460.
(10) Padilha, L. A.; Fu, J.; Hagan, D. J.; Van Stryland, E. W.; Cesar, C. L.; Barbosa, L. C; Cruz, C. H. B.; Buso, D.; Martucci, A. *Phys. Rev. B* **2007**, *75*, No. 075325.
(11) Qu, Y. L.; Ji, W. *J. Opt. Soc. Am. B* **2009**, *26*, 1897.
(12) Schmidt, M. E.; Blanton, S. A.; Hines, M. A.; Guyot-Sionnest, P. *Phys. Rev. B* **1996**, *53*, 12629.
(13) Clapp, A. R.; Pons, T.; Medintz, I. L.; Delehanty, J. B.; Melinger, J. S.; Tiefenbrunn, T.; Dawson, P. E.; Fisher, B. R.; O'Rourke, B.; Mattoussi, H. *Adv. Mater.* **2007**, *19*, 1921.
(14) Hales, J. M.; Hagan, D. J.; Van Stryland, E. W.; Schafer, K. J.; Morales, A. R.; Belfield, K. D.; Pacher, P.; Kwon, O.; Zojer, E.; Bredas, J. L. *J. Chem. Phys.* **2004**, *121*, 3152.
(15) Kang, I.; Wise, F. W. *J. Opt. Soc. Am. B* **1997**, *14*, 1632.
(16) Hines, M. A.; Scholes, G. D. *Adv. Mater.* **2003**, *15*, 1844.
(17) Cademartiri, L.; Montanari, E.; Calestani, G.; Migliori, A.; Guagliardi, A.; Ozin, G. A. *J. Am. Chem. Soc.* **2006**, *128*, 10337.
(18) Xu, C.; Webb, W. W. *J. Opt. Soc. Am. B* **1996**, *13*, 481.
(19) Sheik-Bahae, M.; Said, A. A.; Wei, T. H.; Hagan, D. J.; Van Stryland, E. W. *IEEE J. Quantum Electron.* **1990**, *26*, 760.
(20) Ricard, D.; Roussignol, P.; Flytzanis, C. *Opt. Lett.* **1985**, *10*, 511.
(21) For $\chi^{(3)}$, and consequently 2PA, the local field correction is to the fourth power, that is, $\delta_{2PA} = [1/(f^2|f|^2)]\delta_{2PA,eff}$.
(22) Nootz, G.; Padilha, L. A.; Olszak, P. D.; Webster, S.; Hagan, D. J.; Van Stryland, E. W.; Levina, L.; Sukhovatkin, V.; Brzozowski., L.; Sargent, E. H. *Nano Lett.* **2010**, *10*, 3577.
(23) Hutchings, D. C.; Van Stryland, E. W. *J. Opt. Soc. Am. B* **1992** *9*, 2065.
(24) Negres, R. A.; Hales, J. M.; Kobyakov, A.; Hagan, D. J.; Van Stryland, E. W. *IEEE J. Quantum Electron.* **2002**, *38*, 1205.